Supplementary material

Detecting large-scale networks in the human brain using high-density electroencephalography

Quanying Liu[1,2,3], Seyedehrezvan Farahibozorg[3,4], Camillo Porcaro[2,5,6],

Nicole Wenderoth[1,2], Dante Mantini[1,2,3]

[1] Neural Control of Movement Laboratory, ETH Zurich, 8057 Zurich, Switzerland;

[2] Laboratory of Movement Control and Neuroplasticity, KU Leuven, 3001 Leuven, Belgium;

[3] Department of Experimental Psychology, Oxford University, Oxford OX1 3UD, United Kingdom;

[4] MRC Cognition and Brain Sciences Unit, Cambridge CB2 7EF, United Kingdom;

[5] LET'S-ISTC-CNR, Fatebenefratelli Hospital, 00186 Rome, Italy;

[6] Department of Information Engineering, Marche Polytechnic University, 60131 Ancona, Italy.

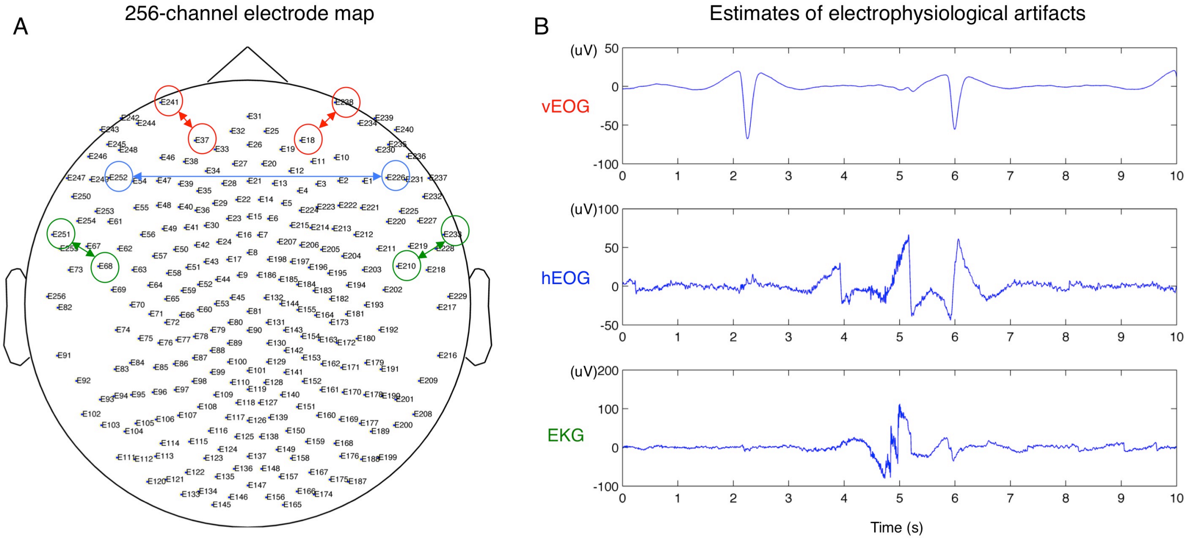

Supplementary Fig. 1 – Example of bio-electrophysiological noise signals. By linearly combining EEG signals collected from a 256-channel system (A) we obtained the vertical electrooculogram (vEOG), the horizontal electrooculogram (hEOG) and the electromyogram (EMG) (B).

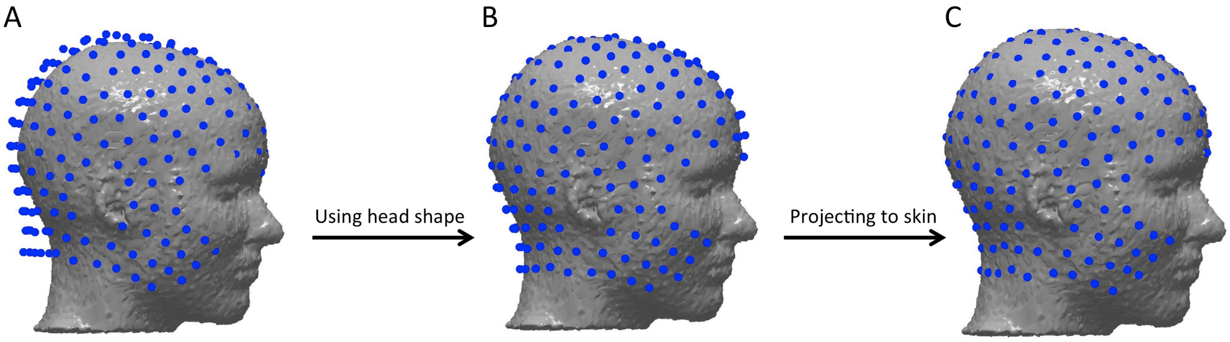

Supplementary Fig. 2 – Electrodes co-registration with individual MR image. (A) matching the three landmarks in electrode space with the three landmarks in individual MRI space; (B) using a rigid transformation to match the head shape extracted from the structural MR image with the shape of EEG sensors; (C) projecting the electrodes onto the surface of the head.

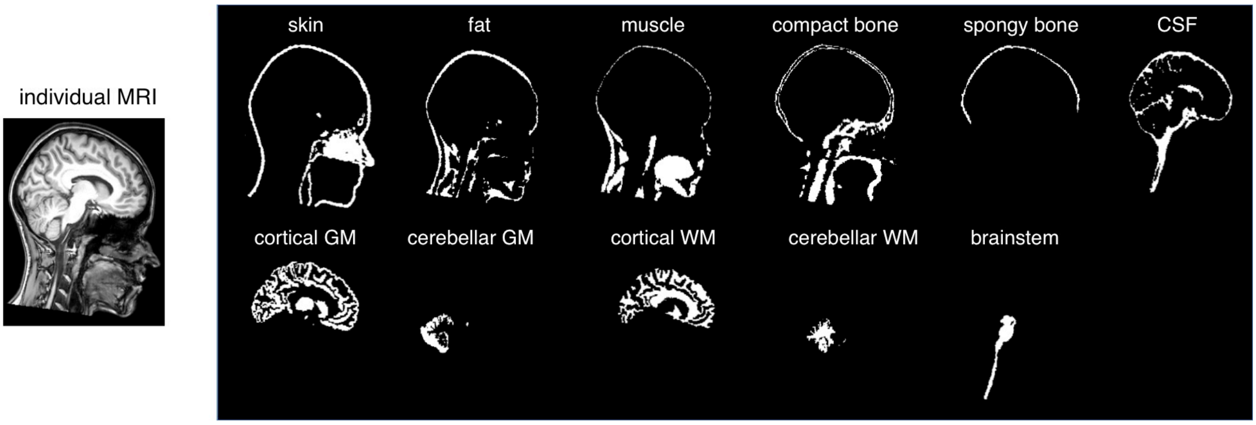

Supplementary Fig. 3 – Example of head tissue segmentation using a template warping approach. The MR image of the subject's head is segmented in 12 compartments: skin, fat, muscle, compact bone, spongy bone, cerebrospinal fluid (CSF), cortical gray matter (GM), cerebellar gray matter, cortical white matter (WM), cerebellar white matter, brain stem, and eyes. An individual MR image is shown in the sagittal section, along with the segmented compartments. Note that eyes are not shown, because they are not visible in the selected MR slice.

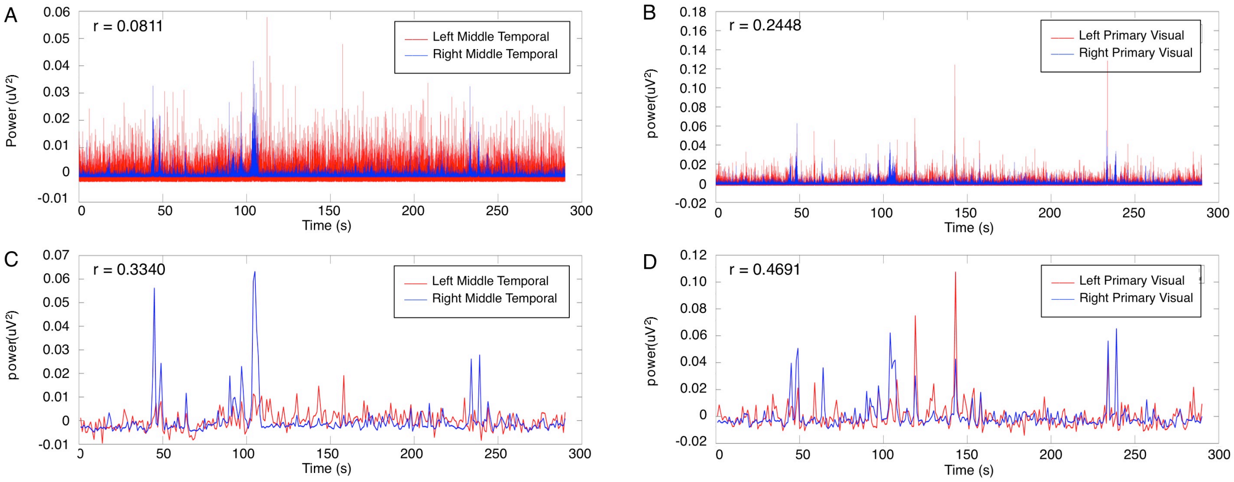

Supplementary Fig. 4 – Effect of power envelope downsampling on connectivity detection. We extracted power time series in wideband (1-80Hz) for brain voxels (A) in the left and right middle temporal area, respectively (MNI coordinates: [-43, -72, -8] and [42, -70, -11]), and (B) in the left and right primary visual area respectively (MNI coordinates: [-3, -101, -1] and [11, -88, -4]). We then downsampled the same power time series to 1 Hz (C-D), and examined the temporal correlation between homologous areas before and after downsampling. Notably, this procedure allowed the detection of connectivity that was not observable from the original data.

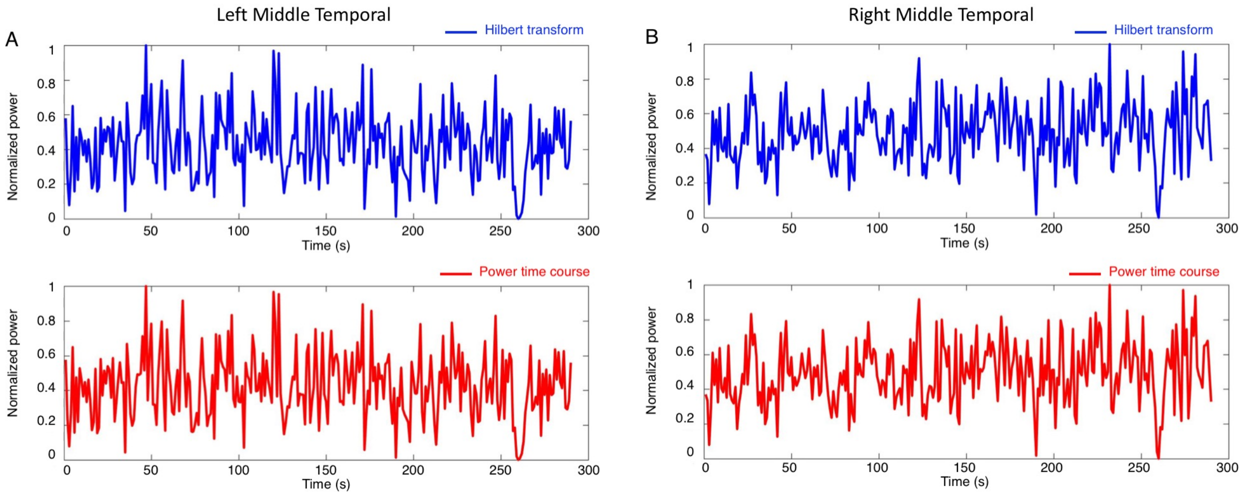

Supplementary Fig. 5 – Comparison of different methods to estimate power envelopes. We extracted neuronal activity in alpha band (8-13Hz) in the left (A) and right (B) middle temporal area, respectively (MNI coordinates: [-43, -72, -8] and [42, -70, -11]). We calculated power envelopes by using the Hilbert transform used in Brookes et al. (2011) (blue) and the moving average approach used in de Pasquale et al. (2010) (red). The correlation between the two estimates for the left and right middle temporal area was equal to 0.995 and 0.997, respectively.

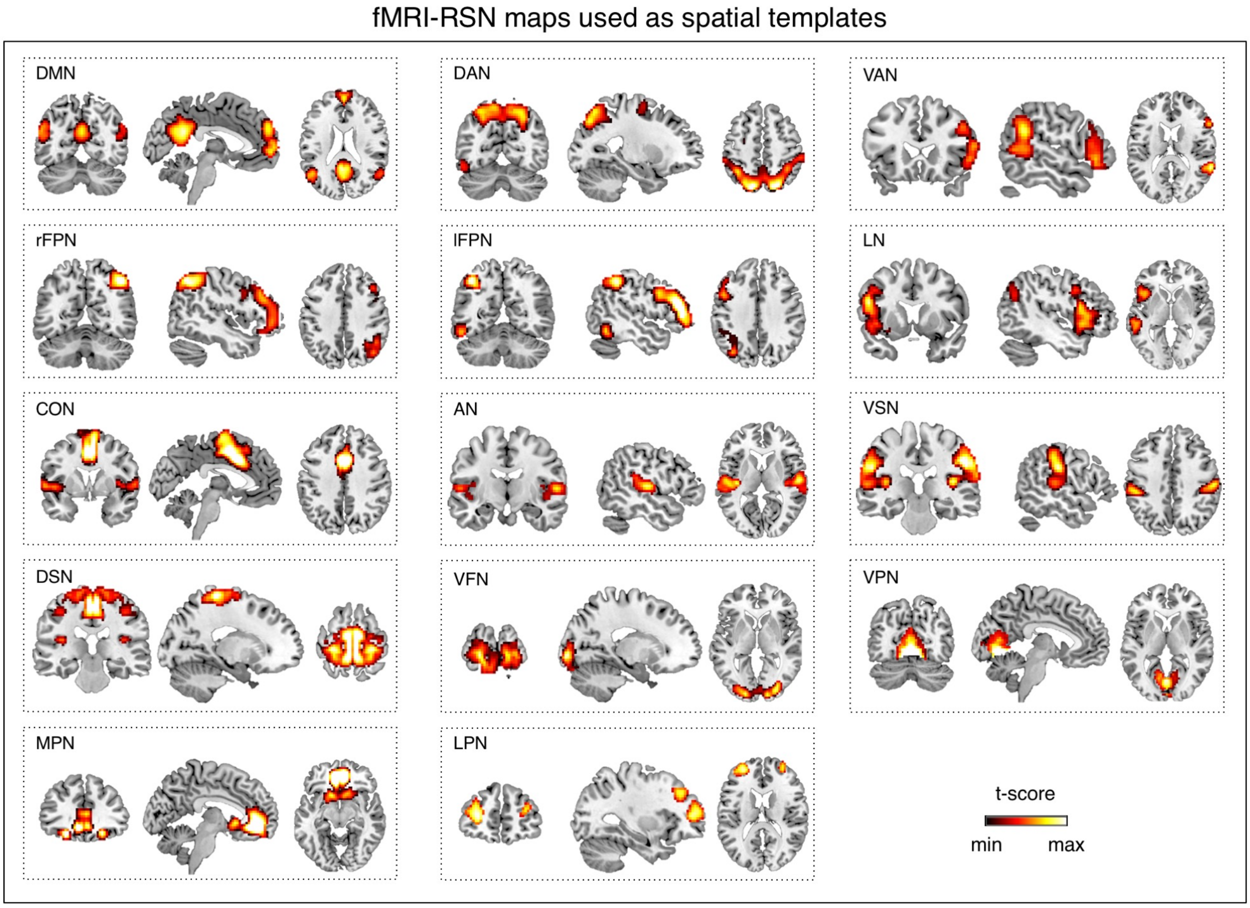

Supplementary Fig. 6 – Fourteen fMRI-RSNs maps used as templates in this study. The maps were obtained from twenty-four healthy subjects at rest (Mantini et al., 2013).

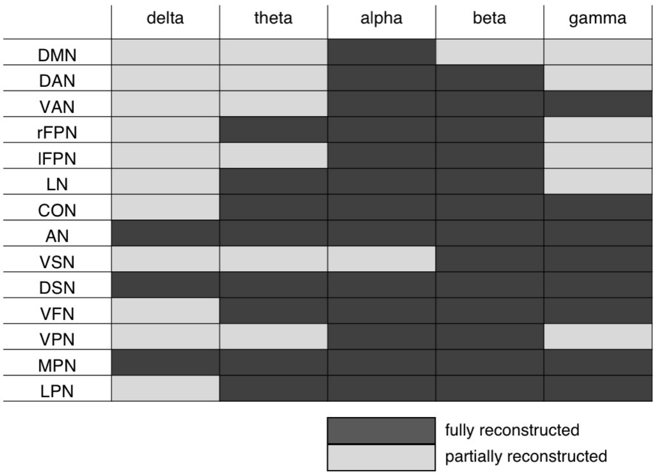

	delta	theta	alpha	beta	gamma
DMN	□	□	■	□	□
DAN	□	□	■	■	□
VAN	□	□	■	■	■
rFPN	□	■	■	■	□
lFPN	□	□	■	■	□
LN	□	■	■	■	□
CON	□	■	■	■	■
AN	■	■	■	■	■
VSN	□	□	□	■	■
DSN	■	■	■	■	■
VFN	□	■	■	■	■
VPN	□	□	■	■	□
MPN	■	■	■	■	■
LPN	□	■	■	■	■

■ fully reconstructed
□ partially reconstructed

Supplementary Fig. 7 – RSN detection for hdEEG data filtered in selected frequency bands. We extracted band-limited power envelopes from source-space signals filtered in the following frequency bands: delta (1-4 Hz), theta (4-8 Hz), alpha (8-13 Hz), beta (13-30 Hz) and gamma (30-80 Hz). We then attempted to reconstruct 14 RSNs by tICA for each frequency band. Finally, we evaluated whether the RSN maps could be fully or only partially reconstructed.

A EEG-RSN maps obtained using temporal ICA: whole-brain source localization

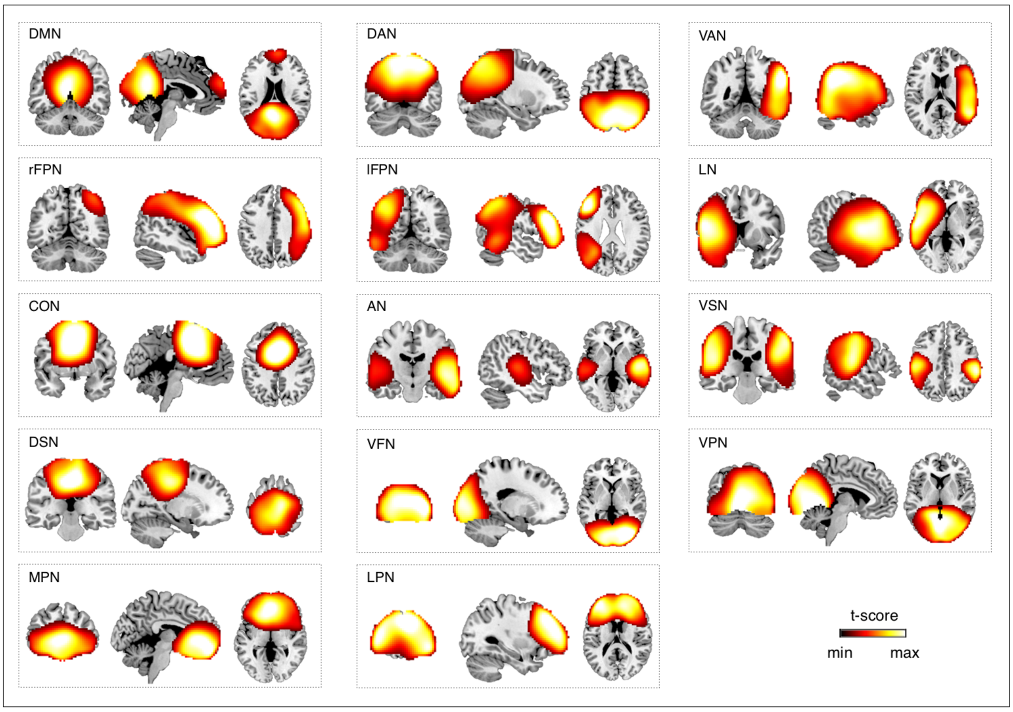

B EEG-RSN maps obtained using spatial ICA: whole-brain source localization

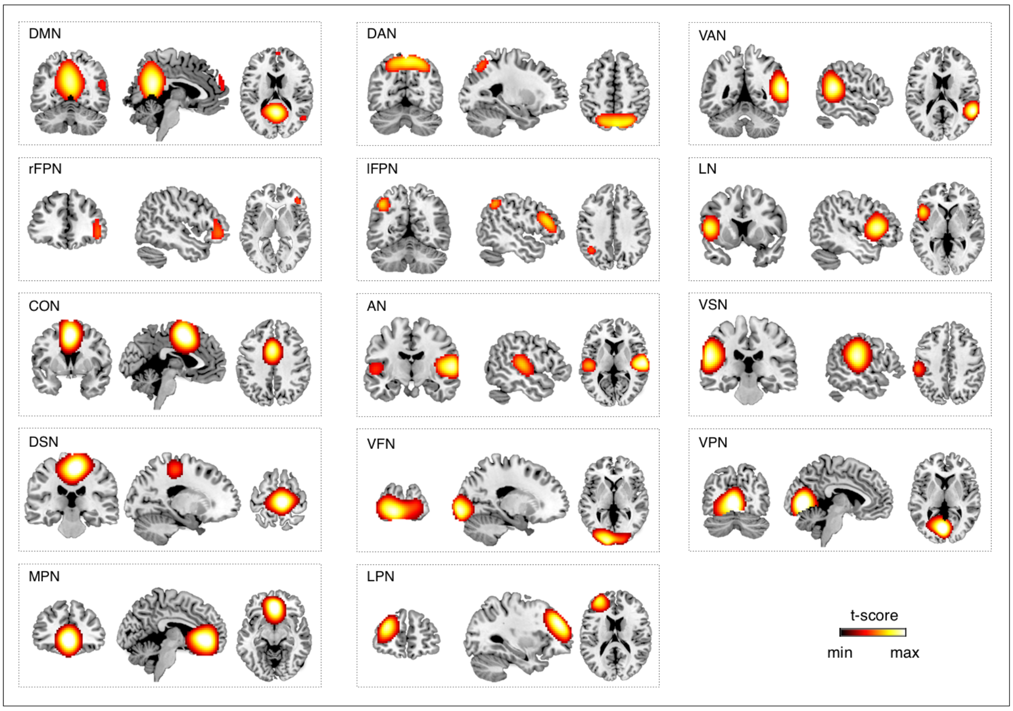

Supplementary Fig. 8 – Comparison of EEG-RSN maps reconstructed using tICA and sICA on whole-brain source space data. RSN detection was performed by using tICA (A) and sICA (B) on source-space data reconstructed in the whole-brain instead of the grey matter only. EEG networks were selected and labeled on the basis of the spatial overlap with fMRI networks: Group-level RSN maps (N=19) were thresholded at $p<0.01$ TFCE-corrected.

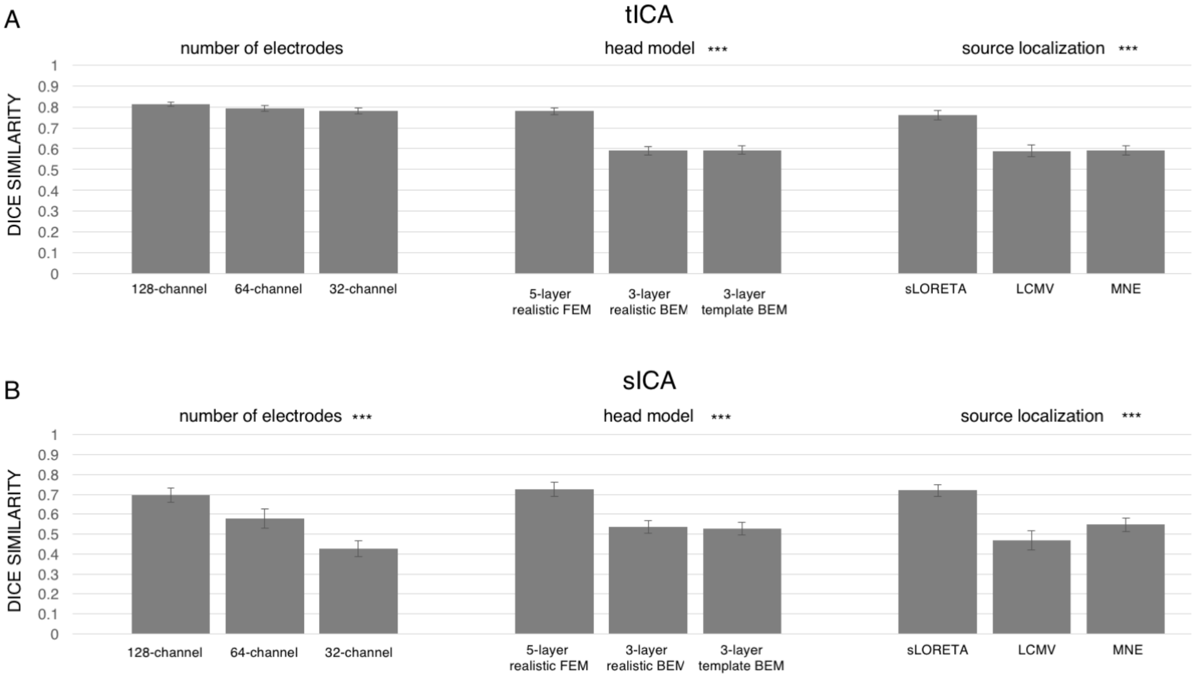

Supplementary Fig. 9 – Impact of the number of EEG channels, the accuracy of the head model and source localization algorithm on EEG-RSN detection by tICA and sICA, respectively. We defined the EEG-RSNs obtained with default settings as reference, and calculated the dice similarity with the corresponding RSNs calculated using different settings. (A) For temporal ICA, we examined the impact of EEG montage density by comparing the maps obtained from 256-channel recordings with those obtained from 128-, 64- and 32-channel recordings; the impact of head modelling by comparing the maps obtained by using a 12-layer FEM with those obtained by 5-layer realistic FEM, 3-layer realistic boundary element model (BEM) and 3-layer template BEM; and the impact of source localization by comparing the maps for eLORETA with those obtained by sLORETA, LCMV and MNE. (B) We repeated the analyses for the maps obtained by sICA. Statistical analyses were conducted using one-way ANOVAs (* for $p<0.05$, ** for $p<0.01$, *** for $p<0.001$).

Supplementary Table 1. Thresholds used for the automated detection of artifactual ICs. These were set in accordance with previous EEG/MEG studies (de Pasquale et al., 2010; Mantini et al., 2009).

Parameter	Threshold value
c_p	0.2
r^2	0.5
k	15

Supplementary Table 2. Conductivity values of different tissues used for the calculation of the head model. The conductivity values associated with the tissue classes were extracted from relevant literature (Haueisen et al., 1997).

Tissue name	Conductivity (S/m)
Skin	0.4348
compact bone	0.0063
spongy bone	0.0400
CSF	1.5385
cortical gray matter	0.3333
cerebellar gray matter	0.2564
cortical white matter	0.1429
cerebellar white matter	0.1099
brainstem	0.1538
eyes	0.5000
muscle	0.1000
fat	0.0400

References

Brookes, M.J., Woolrich, M., Luckhoo, H., Price, D., Hale, J.R., Stephenson, M.C., Barnes, G.R., Smith, S.M., Morris, P.G., 2011. Investigating the electrophysiological basis of resting state networks using magnetoencephalography. Proc Natl Acad Sci U S A 108, 16783-16788.

de Pasquale, F., Della Penna, S., Snyder, A.Z., Lewis, C., Mantini, D., Marzetti, L., Belardinelli, P., Ciancetta, L., Pizzella, V., Romani, G.L., Corbetta, M., 2010. Temporal dynamics of spontaneous MEG activity in brain networks. Proc Natl Acad Sci U S A 107, 6040-6045.

Haueisen, J., Ramon, C., Eiselt, M., Brauer, H., Nowak, H., 1997. Influence of tissue resistivities on neuromagnetic fields and electric potentials studied with a finite element model of the head. IEEE Trans Biomed Eng 44, 727-735.

Mantini, D., Corbetta, M., Perrucci, M.G., Romani, G.L., Del Gratta, C., 2009. Large-scale brain networks account for sustained and transient activity during target detection. Neuroimage 44, 265-274.

Mantini, D., Corbetta, M., Romani, G.L., Orban, G.A., Vanduffel, W., 2013. Evolutionarily novel functional networks in the human brain? Journal of Neuroscience 33, 3259-3275.